Complex multiphase organohydrogels with programmable mechanics toward adaptive soft-matter machines

Shuyun Zhuo[1]*, Ziguang Zhao[1,2]*, Zhexin Xie[3]*, Yufei Hao[3]*, Yichao Xu[1,2], Tianyi Zhao[1], Huanjun Li[4], Elias M. Knubben[5], Li Wen[2,3,6]†, Lei Jiang[1], Mingjie Liu[1,2,6,7]†

Many biological organisms can tune their mechanical properties to adapt to environments in multistable modes, but the current synthetic materials, with bistable states, have a limited ability to alter mechanical stiffness. Here, we constructed programmable organohydrogels with multistable mechanical states by an on-demand modular assembly of noneutectic phase transition components inside microrganogel inclusions. The resultant multiphase organohydrogel exhibits precisely controllable thermo-induced stepwise switching (i.e., triple, quadruple, and quintuple switching) mechanics and a self-healing property. The organohydrogel was introduced into the design of soft-matter machines, yielding a soft gripper with adaptive grasping through stiffness matching with various objects under pneumatic-thermal hybrid actuation. Meanwhile, a programmable adhesion of octopus-inspired robotic tentacles on a wide range of surface morphologies was realized. These results demonstrated the applicability of these organohydrogels in lifelike soft robotics in unconstructed and human body environments.

INTRODUCTION

The complexity and changeability of living environments often require biological organisms to adapt by altering their mechanical properties (1). For example, sea cucumbers can reversibly tune their mechanics through the cross-linking interactions among adjacent collagen fibrils, which significantly affects the strength of the viscoelastic matrix inside the multiphase dermis (2). Intrigued by this capability, bioinspired engineering attempts to blend this intelligent characteristic with artificial materials. With tunable mechanics, artificial materials can offer a promising opportunity for practical applications, including soft-matter machines, biomedical engineering, and wearable devices (3–5). These materials are primarily based on stimuli-responsive polymers (6–9), phase change materials (10, 11), and electric/magnetic rheological systems (12, 13). Reversible mechanical switching between low and high moduli is obtained through responsive cross-linking between a polymer matrix and incorporated fibrils or the rearrangement of nanoparticles under external electric/magnetic fields (14, 15). However, state-of-the-art mechanical tunable materials only have bistable mechanical states: rigid and soft. To date, the development of mechanical programmable materials with multistable states remains challenging.

Here, we report a complex multiphase assembly strategy to fabricate organohydrogels with multistable mechanical states, where phase-transition microrganogel inclusions were incorporated into continuous elastic hydrogel networks. Through an on-demand modular assembly of noneutectic phase transition components within the microrganogel inclusions, our organohydrogels displayed stepwise switching (i.e., triple, quadruple, and quintuple switching) mechanics with multistable modulus plateaus. Furthermore, soft-matter machines, including soft gripper and octopus-inspired tentacles, were developed using these mechanical programmable organohydrogels to achieve high adaptability to complex environments. "Smart" grasping with stiffness matching property and programmable adhesion on a wide range of surface morphologies was realized by regulating the thermal-induced modulus switching of the organohydrogel-based soft machines. Meanwhile, on the basis of the supramolecular interactions of organohydrogel heteronetworks, organohydrogel-based soft machines had promising self-healing capacity, enhancing their tolerance to damage in unpredictable environments.

RESULTS

Complex multiphase modular assembling

Current stiffness-tunable soft-matter machines are primarily based on mechanical tunable materials with bistable states (3). For example, shape memory polymers (16), phase change composites (17–19), and granular jamming (20) have been successfully applied in soft machines to achieve switchable mechanics. However, most soft machines still have inferior adaptability to adjust their mechanical properties to varying targets in working environments. The development of soft-matter machines and the demand for high degrees of adaptability to complex, unconstructed environments require soft materials with programmable multistable mechanics (21–23).

To synthesize these mechanical programmable materials, we proposed a complex multiphase assembly strategy to incorporate reversible interactions as independent functional units in a combined network. The idea was inspired by a multiphase synergetic network that reversibly alters stiffness in biological organisms. Here, long-chain n-alkenes serving as functional modules were macroassembled in an oleophobic poly(stearyl methacrylate) (PSMA)

[1]Key Laboratory of Bio-Inspired Smart Interfacial Science and Technology of Ministry of Education, School of Chemistry, Beihang University, Beijing 100191, P. R. China. [2]Beijing Advanced Innovation Center for Biomedical Engineering, Beihang University, Beijing 100191, P. R. China. [3]School of Mechanical Engineering and Automation, Beihang University, Beijing 100191, P. R. China. [4]School of Chemistry and Chemical Engineering, Beijing Institute of Technology, Beijing 100081, P. R. China. [5]Leitung Corporate Bionic Department, Festo AG & Co. KG, Esslingen 73734, Germany. [6]International Research Institute for Multidisciplinary Science, Beihang University, Beijing 100191, P. R. China. [7]Research Institute of Frontier Science, Beihang University, Beijing 100191, P. R. China.
*These authors contributed equally to this work.
†Corresponding author. Email: liumj@buaa.edu.cn (M.L.); liwen@buaa.edu.cn (L.W.)

network. Both *n*-alkenes and PSMA network have intrinsic phase transition properties with specific crystallization/melting temperatures. As shown in Fig. 1, we modularly assembled multiple oleophilic phase transition components in a hydrophilic network to fabricate complex multiphase organohydrogels with switchable properties. A mixed oil phase including SMA, ethylene glycol dimethacrylate (EGDMA) cross-linker, and *n*-alkanes [i.e., *n*-hexadecane ($C_{16}H_{34}$), *n*-octadecane, and *n*-octacaines ($C_{28}H_{58}$), …] was uniformly dispersed in an aqueous phase of acrylic acid (AA), acrylamide (AM), and nanocross-linker AlOOH nanoparticles (ANPs; diameter, ~3 nm) (Fig. 1A and fig. S1) to prepare an oil-in-water emulsion. The resulting emulsion was stabilized through the Pickering effect of ANPs on the oil/water interface (*24*). During an in situ ultraviolet (UV) gelation process, the emulsion formed organohydrogel heteronetworks that incorporated the uniform distribution of microrganogel inclusions into the hydrogel matrix (Fig. 1B and fig. S2). The spatially heterogeneous structure of the organohydrogels was visualized using confocal laser scanning microscopy, as shown in Fig. 1C, where the continuous hydrogel matrix is shown in blue and the monodispersed microrganogel inclusions with diameters of 2 to 5 µm are shown in orange. The hydrogel network with hydrogen bonding cross-linking synergistically interacted with the microrganogel inclusions of strong hydrophobic associations and crystallization-melting transitions. This synergistic interaction contributed to the formation of a multiphase organohydrogel heteronetwork. Notably, in these microrganogel inclusions, multiple oleophilic components with independent phase transitions were effectively integrated, further eliciting multistage thermoresponsive performance.

Noneutectic multistage phase transitions

Avoiding the eutectic crystallization of oleophilic phase transition components was essential for realizing a multistage switchable property of organohydrogels. Here, *n*-alkanes with significantly different alkyl chain lengths were modularly assembled into the microrganogel inclusions, as shown in Fig. 1B. These well-designed noneutectic oleophilic components can form single-component crystalline solids and individually melt at their own phase transition temperatures (*25–28*), leading to a noninterfering phase transition behavior at the melting/crystallization temperature of each component. For example, as temperature increased above the melting temperature (T_m) of these oleophilic components, the crystallinity of the microrganogel inclusions decreased stepwise from a completely crystalline state to a fully melting state. Consequently, on the basis of these noneutectic components of the microganogels, the organohydrogels can undergo a programmable multistage phase transition.

Here, the modular assembly of $C_{16}H_{34}$ and $C_{28}H_{58}$ (acting as the oleophilic dispersion phase) and PSMA (acting as the oleophilic polymer network) provided noneutectic triple-phase transitions to these microrganogels (Fig. 1D). As shown in fig. S3A, wide-angle x-ray scattering (WAXS) peak positions showed the triclinic geometry of $C_{28}H_{58}$ and $C_{16}H_{34}$ (*29–32*) and paraffin-like hexagonal lattices of PSMA (*33, 34*). On the basis of differences in the crystal structure (d-spacing), alkyl chain lengths and crystallizing temperature, as well as weak interactions between the components, no additional peaks ascribed to eutectic crystals appeared during the crystallization/melting process, indicating a noneutectic property of the microrganogel. Here, we selected three characteristic peaks (20.0° for $C_{16}H_{34}$, 2.9° for PSMA, and 22.5° for $C_{28}H_{58}$) in the WAXS spectra of the organohydrogels

at fully crystalline state (10°C), as shown in Fig. 1E. When the temperature increased to 30°C, the peak at 20.0° disappeared, whereas peaks at 2.9° and 22.5° remained unchanged, resulting from the melting of $C_{16}H_{34}$ at temperatures greater than T_m (18°C). Similarly, peaks at 2.9° and 22.5° vanished as the temperature increased to 50° and 70°C, respectively, due to the individual melting of PSMA ($T_m = 35$°C) and $C_{28}H_{58}$ ($T_m = 57$°C). Gradual crystallization and melting with stepwise transmittance variations were also observed by optical microscope, providing strong evidence of the noneutectic phase transition performance of the microrganogel inclusions over a wide temperature range from 10° to 70°C (fig. S3B). In accordance with the WAXS results, differential scanning calorimeter (DSC) curves confirmed the individual melting/crystallization performance and reversible phase transition property during heating/cooling cycles, as shown in fig. S4. Expectedly, organohydrogels with quadruple- and quintuple-phase transitions also revealed desired multistage noneutectic phase transitions, as shown by WAXS measurements in figs. S5 and S6.

Programmable mechanics with multistable states

Because of the multistage phase transitions of the microrganogel inclusions from rigid solid in the fully crystalline state to viscous liquid in the melting state, the organohydrogels exhibited stepwise switching mechanics. Namely, the organohydrogels with triple-phase transitions that integrated $C_{16}H_{34}$, PSMA, and $C_{28}H_{58}$ inside microrganogel inclusions showed triple-switching mechanics with multiple modulus plateaus (Fig. 2A). The storage modulus (G') of the organohydrogels remained constant at approximately 3.26×10^5 Pa below 15°C and then decreased sharply to 2.13×10^5 Pa as the temperature increased to 20°C. Comparing the variations of G' and DSC thermograms of the organohydrogels, the drop in G' originated from decreased crystallinity of the microrganogel inclusions due to the melting of $C_{16}H_{34}$ at approximately 18°C. The second and third drops in G' occurred at 35° and 58°C, respectively, ascribing to the individual melting of PSMA and $C_{28}H_{58}$. Note that four modulus plateaus were observed between two adjacent phase transitions over wide temperature ranges (<12°C, 18° to 36°C, 44° to 60°C, and >66°C), revealing the multistable mechanics of the organohydrogels. Further compression/tensile tests confirmed the triple-switching mechanics of the organohydrogels. The modulus (E) stepwise decreased from 1.29 to 0.83, 0.33, and 0.10 MPa from 10° to 30°, 45°, and 65°C, respectively, whereas the tensile elongation increased from 20 to 95, 205, and 260% under a constant load of 200 g (Fig. 2A, fig. S7, and table S1). As a result, through the on-demand modular assembly strategy, the organohydrogels with well-designed noneutectic components exhibited quadruple- and quintuple-switching mechanical properties due to the quadruple- and quintuple-phase transitions of the microrganogel inclusions (Fig. 2, B and C; figs. S8 and S9; and tables S2 and S3). Cyclic tests of the storage modulus (fig. S10) and compression modulus (fig. S11) of the organohydrogel material showed that the switching mechanics of the organohydrogel remained stable and repeatable. As the organohydrogel underwent heating-cooling cycles (at 10°, 30°, 45°, and 65°C in sequence), the modulus reversibly switched between four stable states, due to the intrinsic noneutectic crystallization-melting property of the oleophilic components. Therefore, precisely controllable mechanics with multistable states were obtained within the complex multiphase organohydrogels, enabling organohydrogel materials with high programmability.
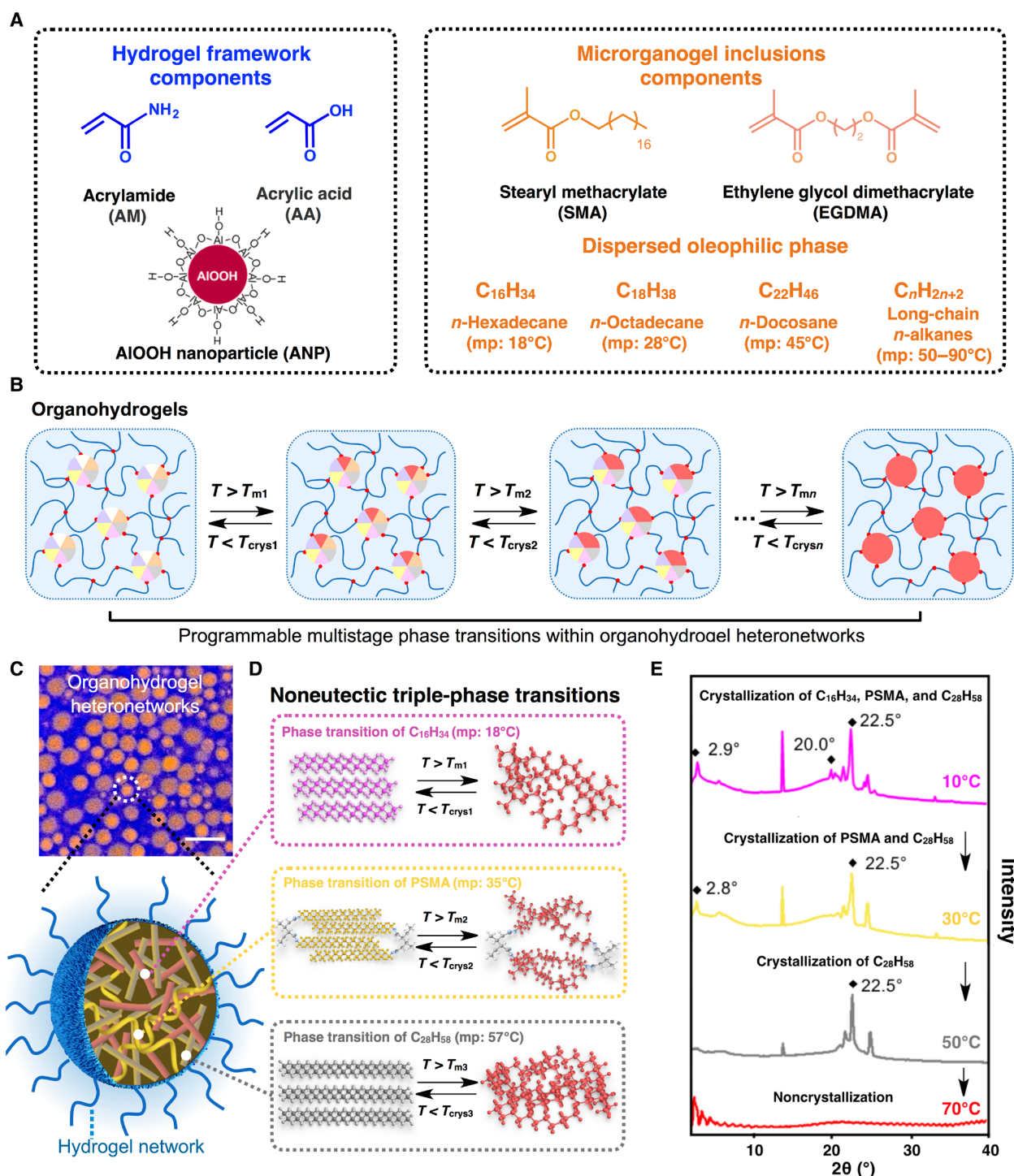
Fig. 1. Design strategy and switching mechanism of the organohydrogels. (**A**) Hydrogel framework components are AA, AM, and ANPs; microrganogel inclusions contain SMA, EGDMA, and n-alkanes. (**B**) Schematic representation of organohydrogels' programmable multiphase transition mechanism that results from the stepwise noneutectic phase transitions of microrganogels through controlling temperature variations. (**C**) Confocal laser scanning microscopy image of the organohydrogel heteronetworks with blue-stained hydrogel framework and orange-stained microrganogel inclusions. Scale bar, 5 μm. (**D**) Illustration showing that the noneutectic triple-phase transitions of organohydrogels. In organohydrogel heteronetwork, these microrganogels contain $C_{16}H_{34}$, PSMA, and $C_{28}H_{58}$, which can melt separately by stepwise temperature controlling. (**E**) Wide-angle x-ray scattering (WAXS) spectra of the organohydrogels demonstrate that the characteristic peaks of $C_{16}H_{34}$, PSMA, and $C_{28}H_{58}$ at 10°C. These peaks disappear sequentially as temperature increases to 70°C, indicating the noneutectic triple-phase transition effect of organohydrogels.
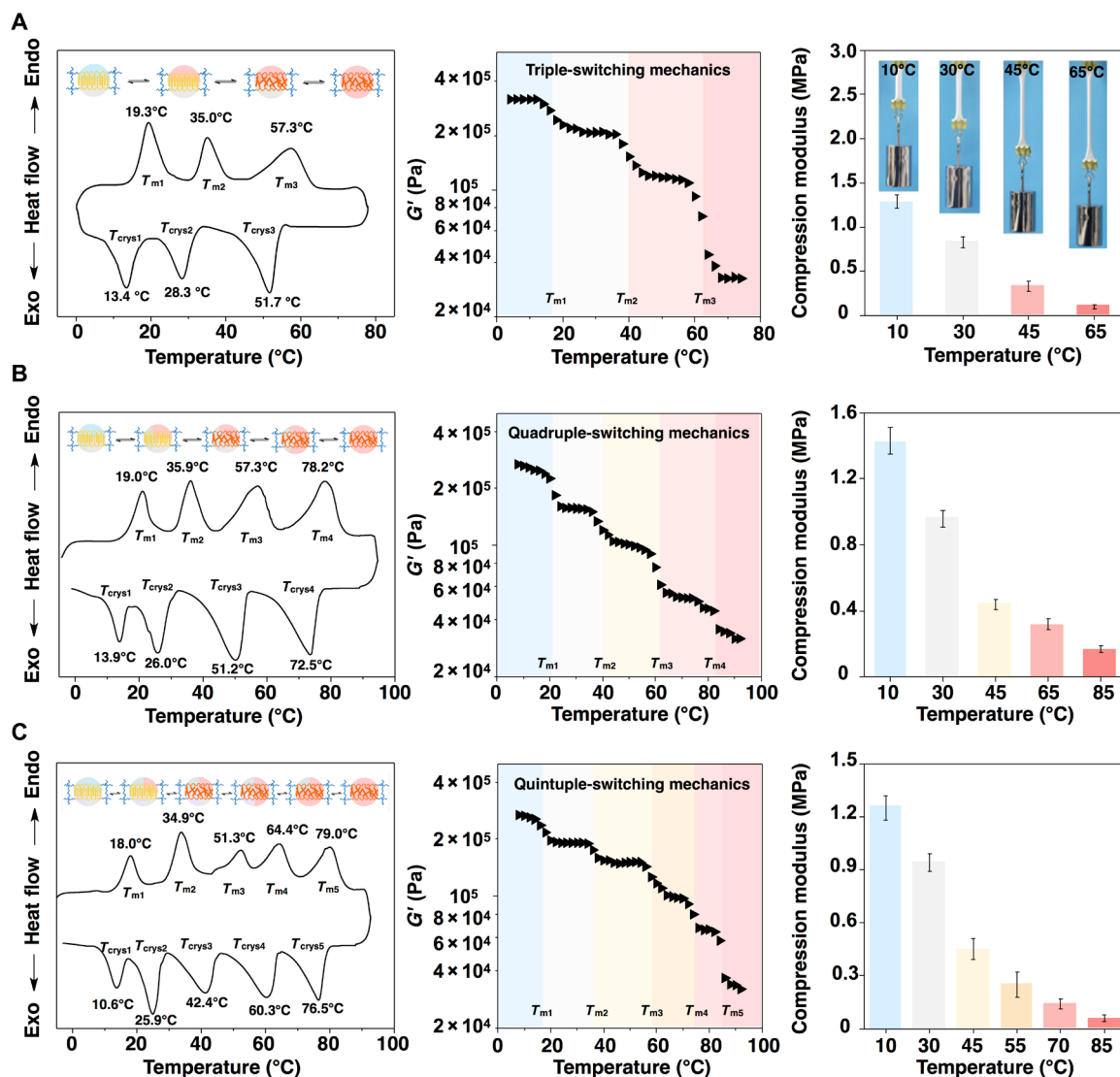
Fig. 2. Precise programmable mechanics with multistable states of the organohydrogels. (**A**) DSC curve of the organohydrogels exhibits three individual melting peaks, demonstrating organohydrogel triple-phase transitions. As a result, the stepwise triple-switching mechanics of organohydrogels can be realized. The inset photos show that programmable organohydrogels with varying applicable mechanical properties through stepwise manipulation of the noneutectic phase transitions in organohydrogels. Scale bar, 1 cm. (Photo credit: Shuyun Zhuo and Ziguang Zhao, Beihang University). (**B** and **C**) Quadruple- and quintuple-switching mechanics of the organohydrogels resulting from multiple modular assembly of corresponding noneutectic phase components within microrganogels. The error bars represent 1 SD ($n = 6$).

Adaptive grasping of the organohydrogel-based soft actuator

The mechanical switchable property of the organohydrogels resembled the stiffness regulation of artificial muscles, which is attractive for soft-matter machines due to their controllability and adaptability to various environments (*35–38*). On the basis of muscle-like switchable mechanics, our organohydrogels have the potential to be used in developing smart soft-matter machines with programmable stiffness adaptations, such as soft robotic grippers (Fig. 3A and fig. S12). Here, we selected organohydrogel materials with triple-switching mechanics to fabricate soft-matter machines (fig. S13). Combining pneumatic actuation, programmable bending with multistable stiffness modulation was realized in a multiphase organohydrogel–based soft gripper. As illustrated in Fig. 3A, this method provided a pneumatic-

thermal hybrid actuation, which is in stark contrast with traditional pneumatic-only methods (figs. S14 and S15). Notably, the bending of the soft gripper originated from thermo-induced modulus switching of the organohydrogels even at constant pneumatic pressure ($P = 12$ kPa) (Fig. 3B and movie S1). The repeated actuation-deactuation experiments showed that the soft gripper can be reversibly operated through the heating-actuating-cooling process (movie S2).

The thermo-induced modulus switching of the organohydrogel materials affected the force output of the gripper (over seven times) (fig. S16 and movie S3); in addition, by appropriately programming the gripper modulus, the gripper was capable of providing delicate grasping when handling very fragile objects. For example, a squishy plasticine ball (elastic modulus, 0.62 MPa) was damaged during the grasping process when operating under pneumatic-only actuation
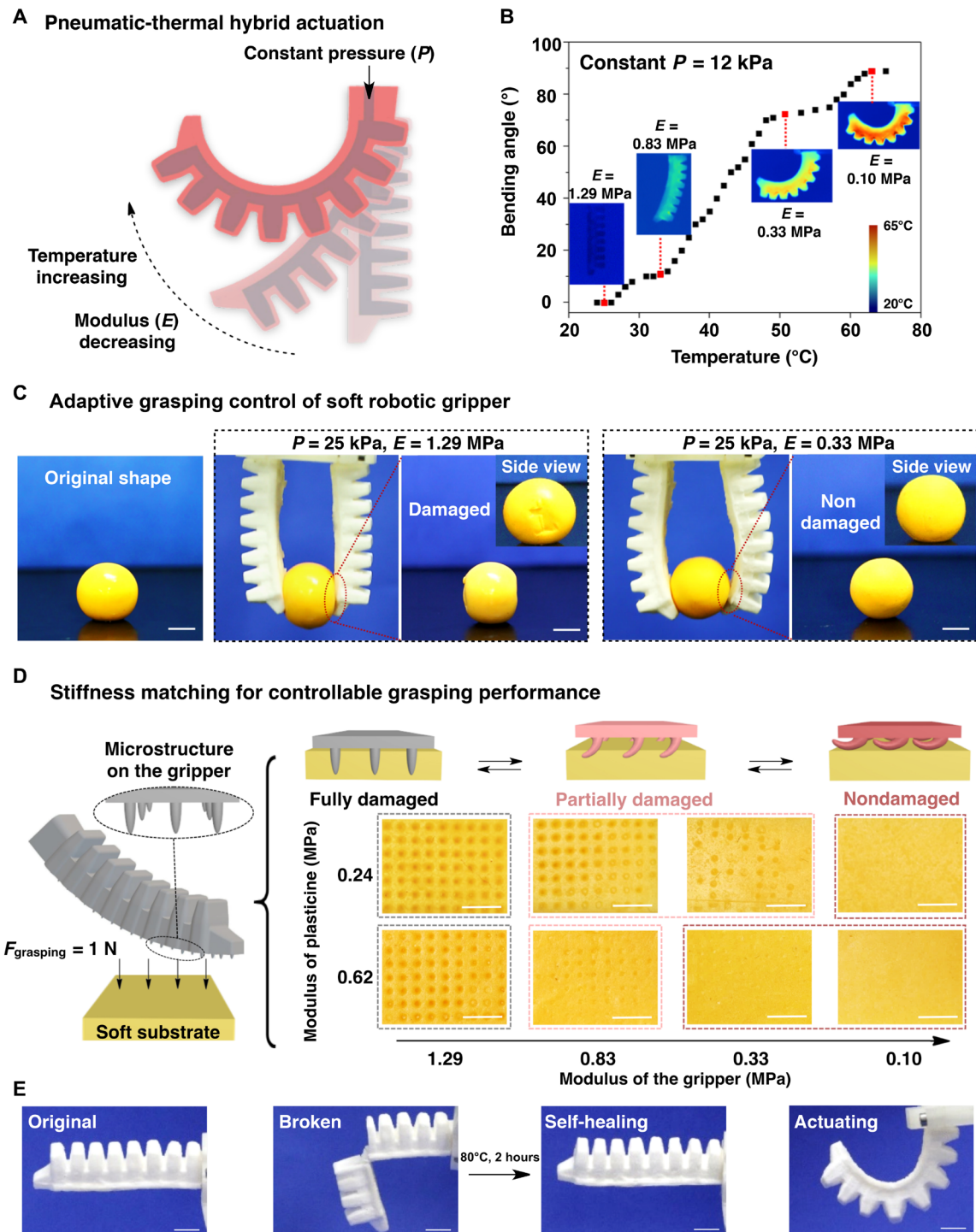
Fig. 3. Adaptive grasping of the soft robotic gripper through pneumatic-thermal hybrid actuation and stiffness matching. (**A**) The illustration exhibits the pneumatic-thermal hybrid actuation of the organohydrogel-based gripper. The bending angle of the gripper increases because of thermal-induced modulus decreasing under constant pressure. (**B**) The bending angles of the gripper at different temperatures. The gripper bends to an angle of 90° as the temperature increased to 63°C in 3 min. The inset images show the infrared pictures of the gripper. (**C**) Protective grasping is realized through programmably adapting the mechanical properties of the gripper to the target objects. The plasticine ball is damaged during grasping with a rigid gripper (with a modulus of 1.29 MPa) while remains intact with a softened gripper (with a modulus of 0.33 MPa) under electrical stimuli of 18 V and the constant pressure of 25 kPa. (**D**) Controllable grasping can be obtained through matching the stiffness of the gripper and the targets under a constant grasping force of 1 N. As the modulus of the organohydrogel-based gripper decreases to lower than that of the plasticine, the gripper can adapt to the plasticine without damage. (**E**) Self-healing performance of the organohydrogel shell of the soft gripper. After being healed at 80°C for 2 hour, the broken gripper outer shell is actuated to a large bending angle with good airtightness. Scale bars, 1 cm. (Photo credit: Shuyun Zhuo, Yufei Hao and Ziguang Zhao, Beihang University).

(P = 25 kPa, voltage V = 0 V, and organohydrogel-based gripper' elastic modulus E_g = 1.29 MPa), as illustrated in Fig. 3C. Under pneumatic-thermal hybrid actuation, the gripper grasped and maintained the plasticine ball without any damage (P = 25 kPa, V = 18 V, and E_g = 0.33 MPa) (movie S4), indicating that the organohydrogel-based actuator had good adaptability. We examined the pressure (P)–bending angle (α) relationship of the actuator over a wide range of bending cycles (on the 500th, 1000th, 1500th, and 2000th cycle). The results showed that the P-α curves did not substantially change at different temperatures (fig. S17), suggesting the repeatability of organohydrogel material-based soft actuators.

Stiffness matching of the organohydrogel soft gripper

We further investigated the ability of stiffness matching during grasping by regulating E_g under pneumatic-thermal hybrid actuation (fig. S18). As shown in Fig. 3D, when the E_g was greater than the modulus of the substrate (E_s), organohydrogel pillars pierced the plasticine substrate, leading to tight interactions. For example, after applying a constant grasping force of 1 N on the plasticine through the gripper at maximum stiffness (E_g = 1.29 MPa), the pillars pierced the plasticine (E_s = 0.24 MPa), leaving obvious holes on the surface. Notably, the interactions can be regulated as the pillars are more compliant and deformable, leading to protective grasping performance. Mild interactions between the gripper and the object were obtained as the E_g switched to lower than the E_s. Specifically, the plasticines with E_s = 0.62 and 0.24 MPa remained intact at E_g = 0.33 and 0.10 MPa, respectively. Therefore, smart adaptive interactions can be realized when handling objects of various stiffnesses by matching the modulus of the organohydrogel-based gripper with the targets.

Moreover, the strong hydrophobic associations of the microrganogel and reestablishing hydrogen bonds between the surface hydroxyl groups of ANPs and carbonyl groups on PAM-co-PAA chains in the hydrogel matrix contribute to the self-healing property of the organohydrogel. At high temperatures, the accelerated entanglement of polymer chains and the phase transition property of the microrganogel inclusions further enhanced the healing process. As shown in fig. S19 and table S4, scratches on organohydrogel surfaces healed without external force; the mechanical strength recovered to 88% of its original state, revealing the effective self-healing properties of the organohydrogel. As shown in Fig. 3E, the self-healing organohydrogel shell of the soft gripper can be inflated again without air leakage after healing at 80°C for 2 hours in a sealed container, indicating the practical benefits of the self-healing property. Comparison experiments were also conducted to show the influence of the self-healing property on the working life span of the organohydrogel-based soft actuator (fig. S20). A damaged soft finger with an obvious scratch at the tip exploded on the 50th actuation-deactuation cycle, whereas a healed soft gripper remained intact even after 2000 actuation-deactuation cycles. This result indicated that the self-healing capacity can potentially extend the life span of soft robotic actuators.

Adaptive adhesion to rough surfaces

On the basis of these results, soft grippers with stiffness matching capabilities can adapt to various substrates based on programmable multistable mechanics. This allowed us to design smart devices that can conform to rough substrates. Inspired by octopus suckers, we developed organohydrogel-based biomimetic soft suckers with programmable adaptability to stick to flat or curved objects with a wide range of surface roughness (Fig. 4A and fig. S21). To achieve adap-

tive adhesion, we introduced a polypyrrole (PPy) network into the organohydrogel material with a nonsignificant effect on the modulus of the material of the biomimetic suckers (fig. S22). The thermoelectric effect of the PPy nanotransducer was used to modulate sucker mechanical states using analog electrical stimuli (figs. S23 and S24). As illustrated in Fig. 4B, with a constant pneumatic pressure of −60 kPa (depressurization), suckers at a modulus of 1.29 MPa (V = 0 V) failed to stick to very rough surfaces (grooves with depth d = 1.22 mm) due to an inferior deformability. Suckers improved their surface adaptability at a modulus of 0.83 MPa under electrical stimuli of 8 V and conformed with rough surfaces (d = 1.22 mm). The better conformability of biomimetic suckers at lower moduli (0.33 and 0.10 MPa) can be achieved on even rougher surfaces (d = 1.81 and 2.01 mm) under electric stimuli of 10 and 17 V, respectively. As shown in Fig. 4C, the pull-off force of a single biomimetic sucker (diameter, 15 mm) decreased from 3.84 to 0.51 N with increasing surface roughness (R_a from 0 to 200 μm). Programmable adaptive adhesion can be achieved by manipulating the mechanics of the sucker to a more compliant and deformable state to match rough surface morphologies (Fig. 4D and fig. S25). For example, the pull-off force on the surface with R_a = 200 μm reached 3.75 N when the modulus of the sucker (E_{sucker}) decreased to 0.83 MPa. Note that the sucker was able to lift a weight as heavy as 34 times its own weight even at the softest state (V = 17 V).

We implemented an array of these organohydrogel-based biomimetic suckers on an octopus-inspired tentacle, which can bend under pneumatic actuation, to show sticking performance on flat/curved objects with both smooth and rough surfaces (Fig. 4A). This prototype can stick and pick up a cell phone (200 g) and a smooth rubber ball (53 g) at E_{sucker} = 1.29 MPa (V = 0 V) (Fig. 4E and movies S5 and S6). The tentacle prototype without electrical stimuli failed to stick to the top of a rough three-dimensionally (3D) printed resin box (R_a = 1.0 mm and 42 g) and a toy basketball with a curvature of 0.067 mm^{-1} (R_a = 1.8 mm and 65 g) (fig. S26), due to air leakage in the biomimetic suckers. In contrast, robust adhesion on the rough resin box (V = 10 V and E_{sucker} = 0.83 MPa) and the toy basketball (V = 8 V and E_{sucker} = 0.33 MPa) was achieved by thermoelectrically modulating the stiffness of all suckers (Fig. 4F and movies S7 and S8). This octopus-inspired tentacle with organohydrogel-based suckers exhibited good adhesion performance and load compacity on flat/curved objects with smooth and rough surfaces due to the programmable adaptability of the organohydrogels through pneumatic-thermal hybrid actuation.

DISCUSSION

Taking inspiration from mechanically tunable biological organisms, we constructed programmable organohydrogel material with multistable mechanical states through an on-demand modular assembly of noneutectic phase transition components inside microrganogel inclusions. The resultant organohydrogel material exhibited precisely controllable thermo-induced stepwise switching (i.e., triple, quadruple. and quintuple switching) mechanics. These mechanical programmable organohydrogels were applied in soft-matter machines. Through pneumatic-thermal hybrid actuation, soft grippers were imparted with adaptive grasping and stiffness matching with various objects. Furthermore, programmable adhesion on a wide range of surface morphologies was realized in the octopus-inspired tentacles. We anticipate that these multiphase organohydrogel–based healable soft
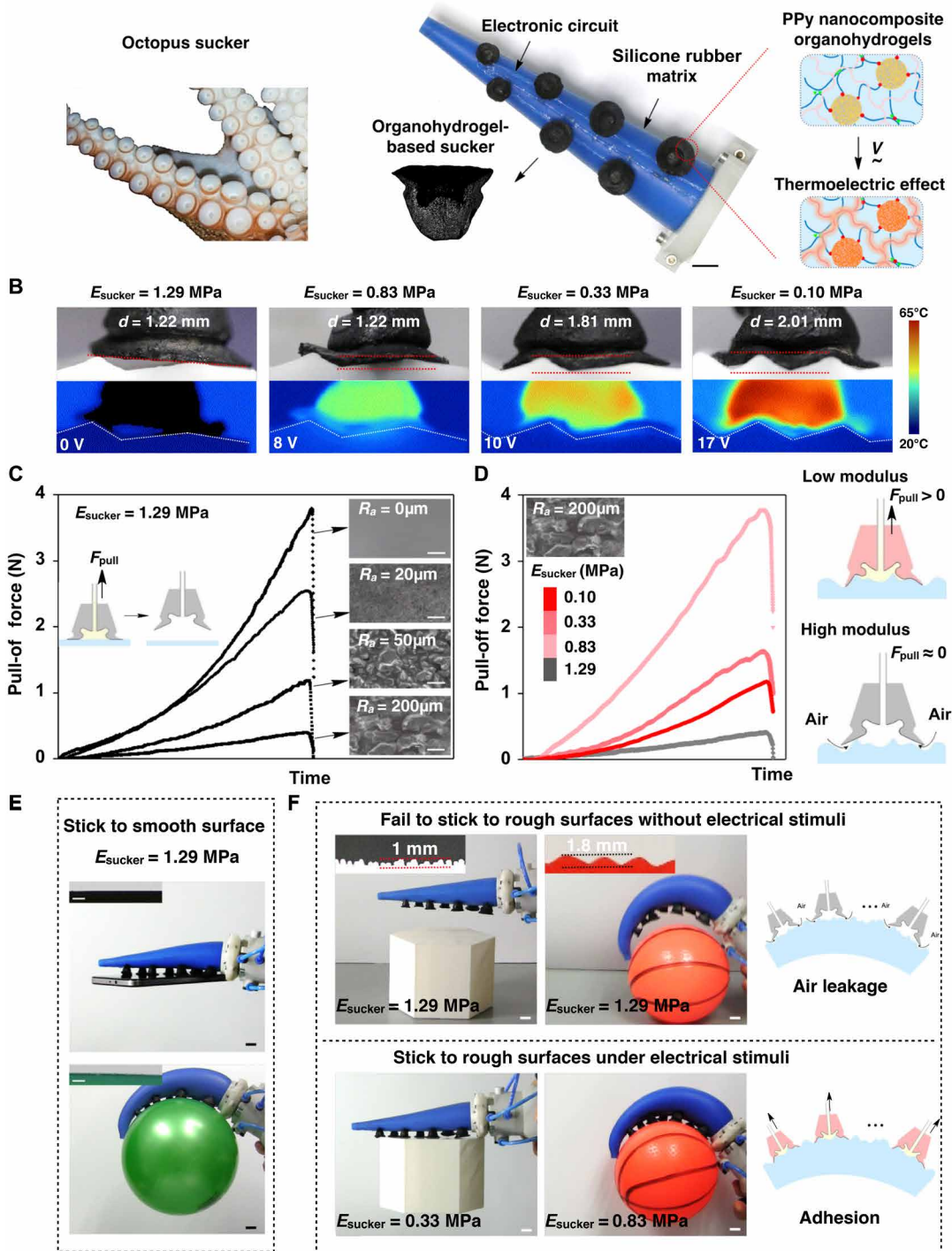
Fig. 4. Programmable adhesion of the octopus-inspired tentacles to rough surfaces. (**A**) Optical images of octopus suckers and the composite octopus-inspired tentacle. Schematic shows the functional organohydrogel-based suckers that integrate the nanotransducer (PPy) with thermoelectric effect into the heteronetworks. (**B**) The suckers with programmable adaptability enable matching various surface morphologies by manipulating the thermoelectric effect. Note that for the specific objects, the suckers can embed into the surfaces to achieve an effective adhesion. (**C**) The pull-off force of a sucker on different rough surfaces (the inset scanning electron microscopy images of surfaces with R_a = 0, 20, 50, and 200 μm; scale bars, 100 μm) under modulus (E_{sucker}) of 1.29 MPa. The unit of the time axis has been normalized for ease of force comparison. (**D**) The pull-off force of a sucker on the surfaces with R_a = 200 μm under different E_{sucker}. The unit of the time axis has been normalized for ease of force comparison. (**E**) When the suckers have a high modulus of 1.29 MPa, the octopus-inspired tentacles can stick to the specific objects with smooth surfaces (inset photos showing the smooth surface morphologies of a phone and a ball; scale bars, 2 mm). (**F**) Programmable adaptability to specific objects with complex rough surfaces can be realized through regulating the sucker' modulus to match surface morphologies (inset photos showing the surface morphologies of a rough resin box and a basketball; scale bars, 1 cm). (Photo credit: Shuyun Zhuo and Zhexin Xie, Beihang University).

machines can promote the development and application of intelligent soft robotics in harsh and complex environments, such as in the human body and underwater.

MATERIALS AND METHODS
Materials
SMA, EGDMA, AM, AA, 2,2′-diethoxyacetophenone (DEOP), Py, iron(III) chloride hexahydrate (FeCl$_3$·6H$_2$O), 4′,6-diamidino-2-phenylindole dihydrochloride, and all n-alkanes (C$_n$H$_{2n+2}$, n = 16, 18, 26, 28, 36, 44, and 50) were purchased from Sigma-Aldrich. Aluminum sol (AlOOH, pseudoboehmite, solid content 20%) was purchased from Suzhou Haipu Hydraulic Equipment Co. Poly (ethylene glycol)–block–poly (propylene glycol)–block–poly (ethylene glycol) [PEG-PPG-PEG; number-average molecular weight (M_n) ~ 12,600, as an emulsifier] was purchased from Aladdin Co. $N,N′$-Bis (2,6-diisopropylphenyl)-1,6,7,12-tetraphenoxy-3,4,9,10-perylenetetracarboxylic diimide (Perylene Red) was purchased from Tokyo Chemical Industry. All the chemicals were used as purchased without further purification. Ecoflex 30 and Mold Star 30 were purchased from Smooth-On Inc., USA. Ni-Cr resistive wire with a diameter of 0.1 mm was bought from www.1688.com.

Methods
Synthesis of the organohydrogels
The organohydrogels were prepared by in situ polymerization of an emulsion. First, 0.50 g of AM, 0.03 g of AA, 0.50 g of aluminum sol, 5 mg of DEOP, and 0.5 mg of PEG-PPG-PEG were added in 1.50 g of water to form an aqueous phase. A mixed oil phase, containing 1.60 g of SMA monomer, 1.60 g of n-hexadecane, 1.20 g of n-octacosane, 6% molar ratio of SMA cross-linker EGDMA, and 5 mg of DEOP, was added to the aqueous phase at 70°C and homogenized at a speed of 18,000 rpm for 5 min to form a stable oil-in-water emulsion. Last, organohydrogels were synthesized from this emulsion by in situ photopolymerization at 60°C for 1.5 hours under the protection of N$_2$.

Likewise, other organohydrogels were prepared using the same procedure. The aqueous phase of all organohydrogels was the same. The oil phase of quadruple-switching organohydrogels consisted of 1.40 g of SMA monomer, 1.10 g of n-hexadecane, 0.90 g of n-octacosane, 0.90 g of n-tetratetracontane, and 6% molar ratio of SMA cross-linker EGDMA. The oil phase of quintuple-switching organohydrogels consisted of 1.10 g of SMA monomer, 0.90 g of n-hexadecane, 0.90 g of n-hexacosane, 0.90 g of n-hexatriacontane, 0.70 g of n-pentacosane, and 6% molar ratio of SMA cross-linker EGDMA.

The oil phase of organohydrogel materials for soft-matter machines consisted of 1.60 g of SMA monomer, 1.60 g of n-octadecane, 1.20 g of n-octacosane, and 6% molar ratio of SMA cross-linker EGDMA. Organogels for measurements were prepared through photoinitiated polymerization of corresponding oil phase mixtures.

Fabrication of soft grippers
The gripper was assembled with finger actuators. A single finger actuator was composed of three parts: a silicone rubber gas cell with an air duct, thin resistive wires with a diameter of 0.1 mm, and the outer gel layer with typical chamber structure. The gas cell was prepared using rubber materials (Ecoflex 30, Smooth-On Inc., USA). Oil-in-water emulsion of gel materials was poured into a polydimethylsiloxane (PDMS) mold, and then, deformed resistive wires and the gas cell were immersed into the emulsion in the right position.

After that, the PDMS mold was put under UV light to initiate the emulsion to polymerize and form the entire finger actuator. The emulsion was viscous so that the resistive wires and gas cell could not sink to bottom. After polymerizing for 2 hours, the resulting finger actuator was taken off from the mold and could be actuated to large bending angles. The bending angles were defined as angles between the connecting lines of two tips at bending state and original straight state.

Fabrication of octopus-inspired smart tentacles
A multistep molding and casting process was used to fabricate the tapered soft actuator with suckers (TSAS) (fig. S21). All the molds for the casting process were designed in SolidWorks and printed using a 3D printer (MakerBot Replicator X5, MakerBot Industries LLC, Hong Kong, China). The molds were assembled and held together firmly with tightly looped rubber rings, while a ring-shaped rod was inserted into the mold to create the core of the robot. Holes were left on the outer mold and threaded with silicone tubes (fig. S21A). Silicone elastomer with 30 Shore A hardness (Mold Star 30, Smooth-On Inc., PA) was poured into the mold (fig. S21B) and degassed in a vacuum chamber for a few minutes. Another 3D printed cap was placed on top of the mold to hold the rod and tubes in place. The elastomer was left for 6 hours at room temperature to cure. After curing, the plastic mold was removed. The rod created a core used for the robot's bending motion, and the tubes were left embedded inside the robot (fig. S21C).

A well-molded PDMS mold for casting the gel suckers was prepared and threaded with two silver wires for the heating of the suckers. Then, the oil-in-water emulsion of the gel materials was poured into the mold (fig. S21E). A cap designed to mimic octopus infundibulum shape was pressed and covered onto the mold, and after that, the mold was put under UV light for 2 hours to initiate the emulsion to polymerize and form the entire sucker. After curing, the mold was removed, and the two silver wires were left inside the sucker for heating. The sucker was first immersed in 0.20 M FeCl$_3$ solution for 4 hours and then immersed in 0.05 M Py solution for 6 hours (fig. S21F). After that, the sucker turned black and conductive because of the PPy network (fig. S21G). The fabricated suckers were well kept in 2 weight % H$_3$PO$_4$ solution, and with the same methods, six more suckers with different sizes were fabricated and mounted on the previously made silicone tentacle (fig. S21C), the silicone tubes threaded the suckers for the vacuum applying, and the silver wires were connected and glued on the surface of the tentacle to form a parallel circuit (fig. S21D). The resultant octopus-inspired tentacle prototype is shown in fig. S21H.

SUPPLEMENTARY MATERIALS
Supplementary material for this article is available at http://advances.sciencemag.org/cgi/content/full/6/5/eaax1464/DC1

REFERENCES AND NOTES

1. P. Egan, R. Sinko, P. R. Leduc, S. Keten, The role of mechanics in biological and bio-inspired systems. *Nat. Commun.* **6**, 7418 (2015).

2. F. Thurmond, J. Trotter, Morphology and biomechanics of the microfibrillar network of sea cucumber dermis. *J. Exp. Biol.* **199**, 1817–1828 (1996).

3. D. Rus, M. T. Tolley, Design, fabrication and control of soft robots. *Nature* **521**, 467–475 (2015).

4. M. A. C. Stuart, W. T. S. Huck, J. Genzer, M. Müller, C. Ober, M. Stamm, G. B. Sukhorukov, I. Szleifer, V. V. Tsukruk, M. Urban, F. Winnik, S. Zauscher, I. Luzinov, S. Minko, Emerging applications of stimuli-responsive polymer materials. *Nat. Mater.* **9**, 101–113 (2010).

5. L. Montero, de Espinosa, W. Meesorn, D. Moatsou, C. Weder, Bioinspired polymer systems with stimuli-responsive mechanical properties. *Chem. Rev.* **117**, 12851–12892 (2017).

6. T. J. White, D. J. Broer, Programmable and adaptive mechanics with liquid crystal polymer networks and elastomers. *Nat. Mater.* **14**, 1087–1098 (2015).

7. A. M. Kloxin, A. M. Kasko, C. N. Salinas, K. S. Anseth, Photodegradable hydrogels for dynamic tuning of physical and chemical properties. *Science* **324**, 59–63 (2009).

8. Z. Zhao, K. Zhang, Y. Liu, J. Zhou, M. Liu, Highly stretchable, shape memory organohydrogels using phase-transition microinclusions. *Adv. Mater.* **29**, 1701695 (2017).

9. J. Reeder, M. Kaltenbrunner, T. Ware, D. Arreaga-Salas, A. Avendano-Bolivar, T. Yokota, Y. Inoue, M. Sekino, W. Voit, T. Sekitani, T. Someya, Mechanically adaptive organic transistors for implantable electronics. *Adv. Mater.* **26**, 4967–4973 (2014).

10. A. Tonazzini, S. Mintchev, B. Schubert, B. Mazzolai, J. Shintake, D. Floreano, Variable stiffness fiber with self-healing capability. *Adv. Mater.* **28**, 10142–10148 (2016).

11. I. M. Van Meerbeek, B. C. Mac Murray, J. W. Kim, S. S. Robinson, P. X. Zou, M. N. Silberstein, R. F. Shepherd, Morphing metal and elastomer bicontinuous foams for reversible stiffness, shape memory, and self-healing soft machines. *Adv. Mater.* **28**, 2801–2806 (2016).

12. H. R. Vutukuri, A. F. Demirörs, B. Peng, P. D. J. van Oostrum, A. Imhof, A. van Blaaderen, Colloidal analogues of charged and uncharged polymer chains with tunable stiffness. *Angew. Chem. Int. Ed.* **51**, 11249–11253 (2012).

13. Z. Varga, G. Filipcsei, M. Zrínyi, Magnetic field sensitive functional elastomers with tuneable elastic modulus. *Polymer* **47**, 227–233 (2006).

14. J. R. Capadona, K. Shanmuganathan, D. J. Tyler, S. J. Rowan, C. Weder, Stimuli-responsive polymer nanocomposites inspired by the sea cucumber dermis. *Science* **319**, 1370–1374 (2008).

15. C. Majidi, R. J. Wood, Tunable elastic stiffness with microconfined magnetorheological domains at low magnetic field. *Appl. Phys. Lett.* **97**, 164104 (2010).

16. A. Firouzeh, J. Paik, An under-actuated origami gripper with adjustable stiffness joints for multiple grasp modes. *Smart Mater. Struct.* **26**, 055035 (2017).

17. S. Rich, S.-H. Jang, Y.-L. Park, C. Majidi, Liquid metal-conductive thermoplastic elastomer integration for low-voltage stiffness tuning. *Adv. Mater. Technol.* **2**, 1700179 (2017).

18. A. Miriyev, G. Caires, H. Lipson, Functional properties of silicone/ethanol soft-actuator composites. *Mater. Design* **145**, 232–242 (2018).

19. J. I. Lipton, S. Angle, R. E. Banai, E. Peretz, H. Lipson, Electrically actuated hydraulic solids. *Adv. Eng. Mater.* **18**, 1710–1715 (2016).

20. Y. S. Narang, J. J. Vlassak, R. D. Howe, Mechanically versatile soft machines through laminar jamming. *Adv. Funct. Mater.* **28**, 1707136 (2018).

21. R. Vaia, J. Baur, Adaptive composites. *Science* **319**, 420–421 (2008).

22. L. Wang, Y. Yang, Y. Chen, C. Majidi, F. Iida, E. Askounis, Q. Pei, Controllable and reversible tuning of material rigidity for robot applications. *Mater. Today* **21**, 563–576 (2018).

23. Y. Wang, X. Yang, Y. Chen, D. K. Wainwright, C. P. Kenaley, Z. Gong, Z. Liu, H. Liu, J. Guan, T. Wang, J. C. Weaver, R. J. Wood, L. Wen, A biorobotic adhesive disc for underwater hitchhiking inspired by the remora suckerfish. *Sci. Robot.* **2**, eaan8072 (2017).

24. W. P. Hohenstein, H. Mark, Polymerization of olefins and diolefins in suspension and emulsion. Part I. *J. Polym. Sci.* **1**, 127–145 (1946).

25. Y.-H. Lee, W.-C. Chen, Y.-L. Yang, C.-J. Chiang, T. Yokozawa, C.-A. Dai, Co-crystallization phase transformations in all π-conjugated block copolymers with different main-chain moieties. *Nanoscale* **6**, 5208–5216 (2014).

26. M. Zhu, S. Pan, Y. Wang, P. Tang, F. Qiu, Z. Lin, J. Peng, Unravelling the correlation between charge mobility and cocrystallization in rod–rod block copolymers for high-performance field-effect transistors. *Angew. Chem. Int. Ed.* **57**, 8644–8648 (2018).

27. S. Pal, A. K. Nandi, Cocrystallization behavior of poly(3-alkylthiophenes): Influence of alkyl chain length and head to tail regioregularity. *Macromolecules* **36**, 8426–8432 (2003).

28. I. D. Rubin, R. D. Pugliese, A study of blends of poly (n-octadecyl methacrylate) with n-dodecane and n-octadecane. *Angew. Chem. Int. Ed.* **171**, 165–173 (1989).

29. S. Dutta, S. K. Prasad, Confinement-driven radical change in a sequence of rotator phases: A study on n-octacosane. *Phys. Chem. Chem. Phys.* **20**, 24345 (2018).

30. D. Fu, Y. Su, X. Gao, Y. Liu, D. Wang, Confined crystallization of *n*-hexadecane located inside microcapsules or outside submicrometer silica nanospheres: A comparison study. *J. Phys. Chem. B* **117**, 6323–6329 (2013).

31. B. Wu, G. Zheng, X. Chen, Effect of graphene on the thermophysical properties of melamine-urea-formaldehyde/N-hexadecane microcapsules. *RSC Adv.* **5**, 74024–74031 (2015).

32. L. P. Wang, Q. F. Li, C. Wang, X. Z. Lan, Size-dependent phase behavior of the hexadecane–octadecane system confined in nanoporous glass. *J. Phys. Chem. C* **118**, 18177–18186 (2014).

33. C. Bilici, O. Okay, Shape memory hydrogels via micellar copolymerization of acrylic acid and *n*-octadecyl acrylate in aqueous media. *Macromolecules* **46**, 3125–3131 (2013).

34. A. Matsuda, J. Sato, H. Yasunaga, Y. Osada, Order-disorder transition of a hydrogel containing an n-alkyl acrylate. *Macromolecules* **27**, 7695–7698 (1994).

35. M. A. McEvoy, N. Correll, Materials that couple sensing, actuation, computation, and communication. *Science* **347**, 1261689 (2015).

36. J. Shintake, V. Cacucciolo, D. Floreano, H. Shea, Soft robotic grippers. *Adv. Mater.* **30**, 1707035 (2018).

37. B. Gorissen, D. Reynaerts, S. Konishi, K. Yoshida, J.-W. Kim, M. De Volder, Elastic inflatable actuators for soft robotic applications. *Adv. Mater.* **29**, 1604977 (2017).

38. J. A. E. Hughes, P. Maiolino, F. Iida, An anthropomorphic soft skeleton hand exploiting conditional models for piano playing. *Sci. Robot.* **3**, eaau3098 (2018).

Citation: S. Zhuo, Z. Zhao, Z. Xie, Y. Hao, Y. Xu, T. Zhao, H. Li, E. M. Knubben, L. Wen, L. Jiang, M. Liu, Complex multiphase organohydrogels with programmable mechanics toward adaptive soft-matter machines. *Sci. Adv.* **6**, eaax1464 (2020).